Origin of soft-mode stiffening and reduced dielectric response in $SrTiO_3$ thin films

T. Ostapchuk, J. Petzelt, V. Železný, A. Pashkin, J. Pokorný, and I. Drbohlav
Institute of Physics, Academy of Sciences of the Czech Republic Na Slovance 2, 182 21 Prague 8, Czech Republic

R. Kužel and D. Rafaja
Faculty of Mathematics and Physics, Charles University, Ke Karlovu 5, 12116 Prague 2, Czech Republic

B. P. Gorshunov* and M. Dressel
Physikalisches Institut, Universität Stuttgart, D-70550 Stuttgart, Germany

Ch. Ohly, S. Hoffmann-Eifert, and R. Waser
Institut f. Festkörperforschung Jülich, D-52425 Jülich, Germany
(Received 17 July 2002; published 13 December 2002)

The problem of the reduced dielectric response in thin films of high-permittivity materials is analyzed by studying the soft-mode response in several $SrTiO_3$ thin films by means of Fourier transform far infrared, monochromatic submillimeter, and micro-Raman spectroscopies. A 300-nm-thick metalorganic chemical vapor deposition film, quasiepitaxially grown on a (0001) sapphire substrate with a perfect ⟨111⟩ orientation, displays a ferroelectric transition near 125 K induced by a tensile residual stress, appearing apparently simultaneously with the antiferrodistortive transition. On the other hand, polycrystalline chemical solution deposition films grown on (0001) sapphire, and also tensile stressed, show a harder soft mode response without the appearance of macroscopic ferroelectricity. This effect, which increases with the film thickness, is explained by a strong depolarizing field induced by the percolated porosity and cracks (in the 10-nm scale) along the boundaries of columnar grains (normal to the probe field direction). Brick-wall model calculations showed that 0.2 vol. % of such a porosity type reduces the permittivity from 30000 to less than 1000. The activation of the forbidden IR modes in the Raman spectra in the whole 80–300-K temperature range studied is explained by the effect of polar grain boundaries, in analogy with the bulk ceramics.

DOI: 10.1103/PhysRevB.66.235406 PACS number(s): 78.30.−j, 77.55.+f, 77.80.−e, 63.20.−e

I. INTRODUCTION

Remarkably high dielectric permittivity, as well as its tunability and low loss at high frequencies, make paraelectric and incipient ferroelectric (FE) materials very attractive for microwave and radio-frequency applications. However, the permittivity of the corresponding thin films, required for device applications, is very sensitive to the film parameters, substrate, and processing, and as a rule is substantially reduced.[1–4] In spite of extensive studies, the understanding of this phenomenon still remains a challenging task for both applied and basic research.

In the present work we have addressed this problem in the case of the perovskite $SrTiO_3$ (STO) thin films. On the one hand, the growing interest in this material is connected with its utilization in high temperature superconductor-dielectric heterostructures,[5,6] on the other hand, its popularity owes much to the discovery of the first polar soft mode behavior in STO crystals[7] and the so called ''Müller state'' at low temperatures.[8] Its simple room-temperature cubic structure ($Pm\bar{3}m-O_h^1, Z=1$) shows a tendency toward two lattice instabilities: an antiferrodistortive (AFD) one, leading to a structural phase transition near $T_a \approx 105$ K, and a FE one, responsible for the incipient ferroelectricity. These two instabilities are connected with two different order parameters and two corresponding soft phonon modes.

The AFD soft mode [triply degenerate $R'_{15}(F_{1g})$] is associated with the antiphase tilting of the TiO_6 octahedra. Its condensation results in a second-order phase transition into a tetragonal ($I4/mcm-D_{4h}^{18}$) phase with the primitive unit cell doubling ($Z_{\text{prim}}=2$). The consequent folding of the Brillouin zone transfers this phonon mode from the R point into the Brillouin-zone center (Γ point). The symmetry reduction splits the triplet into an A_{1g} singlet and an E_g doublet, which harden saturating at about 49 and 15 cm^{-1}, respectively.[9,10] Both components are Raman active but nonpolar and hence infrared (IR) inactive.

Conversely, the FE soft mode (triply degenerate F_{1u}) is polar and Raman inactive. As the strongest IR mode it dominates in the dielectric response. Altogether, the dielectric function of STO consists of contributions of three F_{1u} transverse optic (TO) modes and, unlike most of high-permittivity dielectrics, it does not exhibit any appreciable microwave or lower-frequency dispersion.[11,12] In the order of increasing frequency, the FE soft mode TO1 consists predominantly of Ti-O-Ti bending, TO2 of Sr against TiO_6 octahedra translations, and TO4 of Ti-O stretching.[13,14] TO3 (F_{2u}) is a silent mode, optically inactive. The eigenfrequencies of TO2 (≈ 178 cm^{-1}) and TO4 (≈ 546 cm^{-1}) are practically temperature independent, and their dielectric strengths are almost negligible in comparison with that of the soft TO1 phonon. The fit of the near-normal far IR (FIR) reflectivity reported in Refs. 7 and 15–17 yields a room-temperature value of ω_{TO1} between 87 and 91 cm^{-1}. The low-

temperature soft mode parameters can be hardly determined by the conventional IR reflection technique with high accuracy because ω_{TO1} strongly decreases beyond the reliably measurable FIR range and the reflectivity approaches unity. Moreover, the penetration depth in the soft-mode frequency range is less than 1 μm, so that the results are influenced by the surface layer which is known to differ from the bulk properties in STO crystals[18] as well as in ceramics.[19]

Precise studies of the low-temperature FE soft-mode behavior were recently performed by high-resolution hyper-Raman scattering on single-domain crystals.[20] Below the AFD transition the FE soft-mode triplet splits into an E_u doublet and an A_{2u} singlet, softening down to 7.8 and 16.5 cm^{-1} at the liquid-He temperature, respectively. No minimum, but a leveling off, was found in their temperature dependence, in agreement with the incipient FE instability in STO which does not lead to formation of a macroscopic FE phase. The leveling off was assigned to quantum fluctuations, which become important at low temperatures.[8] Recently the competitive AFD instability was shown to play an even more important role in this effect.[20] Nonetheless, the behavior of the FE soft mode follows the Cochran law ($\omega_{TO1}^2 \approx T - T_C$) above 50 K, with an extrapolated Curie temperature T_C of about 40 K.[20] Inserting its eigenfrequencies into the Lyddane-Sachs-Teller relationships yields the Curie-Weiss temperature dependence (above $\sim$50 K) of the static permittivity, growing from about 300 at room temperature up to $\varepsilon_c \sim 10000$ in the direction parallel to the tetragonal axis, and to $\varepsilon_a \sim 40000$ in the perpendicular direction at the liquid-He temperature. This agrees with the direct dielectric measurements, though ε_a values are somewhat lower—ranging from 25000 to 32000.[21–23]

The lowest-temperature permittivity of STO thin films is usually less than 2000 (e.g., Refs. 1, 2, and 4–6). Wide-frequency range measurements on STO films indicated no appreciable dielectric dispersion,[2,24] so that it is believed that in STO films the dielectric properties are also determined by the FE soft mode dynamics, which should therefore differ from that in single crystals. Indeed, Fedorov *et al.*[17] first demonstrated that the FE soft mode in a polycrystalline STO film ceases to soften and levels off near $\sim$60 cm^{-1} at a temperature corresponding to the AFD transition, and that its effective damping, much larger than in crystals, grows on cooling. A similar incomplete softening of TO1 was observed on highly epitaxial 0.5–2-μm-thick STO films.[25,26] Further studies[27–31] showed that in addition to this common tendency in the temperature dependence, the soft-mode dynamics varies for different films. This phenomenon has not been explained so far, and no clear correlation between any of the STO film characteristics and soft mode and/or lower-frequency dielectric properties has been found.

In this paper we report on the temperature behavior of the FE soft-mode parameters in three STO films differing by the deposition processing, degree of ordering, and thickness, and compare them with the previous results. The dielectric response of the films has been determined using the transmission Fourier transform infrared (FTIR) spectroscopy, which is known to be a powerful tool for the analysis of semiconductor film systems.[32] Utilization of FTIR spectroscopy for studies of the soft-mode dynamics in FE films was demonstrated in Refs. 17, 28, 30, 31, and 33. In these papers mostly a simplified approach of data analysis was used, which neglects interference phenomena due to multiple passages through the substrate. In the present experiment, high-resolution measurements were performed and analyzed using rigorous formulas to resolve the dense interference fringes due to the substrate. These, together with the detailed structural characterization of our films, enabled us to reveal and interpret some effects and find important differences between the behavior of highly oriented and polycrystalline films. It will be shown that the residual stress effect, leading to the FE transition, dominates in the behavior of the quasiepitaxial film, whereas percolated pores and possible cracks, which substantially increase the FE soft-mode frequency and reduce the static permittivity, are dominant factors in the polycrystalline films response.

II. EXPERIMENT

A. Sample processing and characterization

Three STO films (STO1, STO2, and STO3; see Table I) deposited on (0001)-oriented sapphire substrates were studied in the present work. The STO1 film was produced by the injection metalorganic chemical vapor deposition (MOCVD) technique with a substrate temperature of 800 °C and a reactor pressure of 5 Torr. After the deposition, the film was annealed for 30 minutes in the oxygen atmosphere to arrive at the right oxygen content. The detailed film processing is described elsewhere.[34] STO2 and STO3 films were prepared by the chemical solution deposition (CSD) technique.[35] The 0.2 Mol precursor solution (propionate route) was spun onto substrates 18 times for obtaining the thinner STO2 film and 36 times for the thicker STO3 film. Each spinning was followed by annealing at 750 °C for 10 min. Final crystallization was performed at 800 °C for 1 h in oxygen flow (1 bar).

All the studied films possessed a grained structure, but STO1 exhibited a three-dimensional alignment of the crystallites orientation with two in-plane orientations that allowed one to consider it quasiepitaxial and to study its structure by a single-crystal x-ray diffraction (XRD) method using a two-circle diffractometer (Huber) with parallel beam optics. Two other films of a weak texture were studied by the powder difractometer XRD7 (Seifert-FPM).

The STO1 film was found to have a perfect $\langle 111 \rangle$ orientation perpendicular to the sample surface accompanied by a bimodal distribution of the in-plane crystallite orientations: their [110] directions were rotated either $+30°$ or $-30°$ with respect to the [1000] direction of the sapphire substrate.[39] The in-plane grain size, estimated from atomic force microscopy (AFM) surface view, was $\sim$100 nm (Fig. 1).

In order to obtain information about the macroscopic and microscopic lattice deformation, the positions and shapes of the symmetrical 111 and 222 reflections and that of the asymmetrical 211, 322, and 332 reflections were analyzed. The in-plane macroscopic lattice deformation, calculated from the dependence of individual lattice parameters on $\sin^2\psi$ (ψ is the sample inclination from the symmetrical position), was 0.17%. This lattice deformation corresponds to a

TABLE I. Structural and morphological characteristics of the studied films.

Films	STO1	STO2	STO3
Substrate	Al_2O_3 (0001)	Al_2O_3 (0001)	Al_2O_3 (0001)
Deposition method	MOCVD	CSD	CSD
Layer growth	quasi-epitaxial	polycrystalline	polycrystalline
Orientation/texture	perfect ⟨111⟩	weak ⟨100⟩	weak ⟨100⟩
Residual stress	tensile (0.7±0.1) GPa	tensile (0.40±0.05) GPa	tensile (0.15±0.03) GPa
Macroscopic lattice deformation	0.17%	0.10%	0.04%
Microstrain	~0.7%	0.18%	0.18%
In-plane grain size (AFM)	~100 nm	~100 nm	~100 nm
Cross-sectional view (SEM)	–	80–200-nm thick columns; pores (~15 nm diameter)	80–150-nm thick columns; pores (~15 nm diameter)
Thickness	290 nm	360 nm	720 nm
Sr/Ti (RBS)	0.97±0.05	1.05±0.05	0.96±0.05

tensile residual stress of 0.7 GPa (calculated with the Young modulus of 300 GPa). The stress-free lattice parameter a_0 was calculated from the same dependence of lattice parameters as the lattice deformation. For the Poisson ratio of 0.24 (calculated from the single-crystalline elastic constants[38]), we obtained $a_0 = 0.39057$ nm. The microscopic lattice deformation (~0.75 %) was estimated from the broadening of the 332 reflection. Assuming a large crystallite size, the size effect on the line broadening was neglected. A complete description of the XRD experiment performed on the STO1 film and similar MOCVD films of $BaTiO_3$ (BTO) and $Ba_{0.1}Sr_{0.9}TiO_3$ (BST) was given in Ref. 39.

The CSD films STO2 and STO3 turned out to be polycrystalline with a weak ⟨100⟩ texture (the Harris texture index was less than 1.5). The macroscopic residual stress, determined in the same way as for STO1, was also tensile but weaker: 0.4 GPa in STO2 and 0.15 GPa in STO3. Microstrain, dominating in the diffraction line broadening, was found to be 0.18% for both polycrystalline samples. The crystallite size was a minor effect of the line broadening for both films, indicating a rather large grain size in normal direction. The in-plane grain size, estimated from the AFM micrographs, was of about 100 nm for both films (Fig. 2). The AFM micrographs of both polycrystalline films are very similar. In contrast to STO1, their surfaces are much smoother, which may indicate a different energy balance between the surface and grain boundaries of these films. Scanning electron microscopy (SEM) cross-sectional images of the STO2 and STO3 films demonstrate a columnar structure (Fig. 3). The columns, according to the XRD results and previous transmission electron microscopy (TEM) study,[35,36] are single crystalline. As demonstrated in Refs. 35 and 36 the porosity in such films appears prevailingly at the grain boundaries (see Fig. 3, which shows a break along the grain boundaries). The density of these films was estimated by x-ray reflectometry to be about 95%. Film thickness, evaluated using single-crystal refractive index[37] by estimating distances between the interference fringes in optical transmittance spectra, and thickness, obtained from Rutherford backscattering (RBS) on the basis of single-crystal density,[38] agrees with the values estimated from SEM view within a 5% precision. This also indicates rather high density. RBS demonstrated a good stoichiometry of all three films.

B. FIR transmittance measurements

FTIR transmittance measurements (20–400 cm^{-1}) were carried out on a FT interferometer Bruker IFS 113v with a

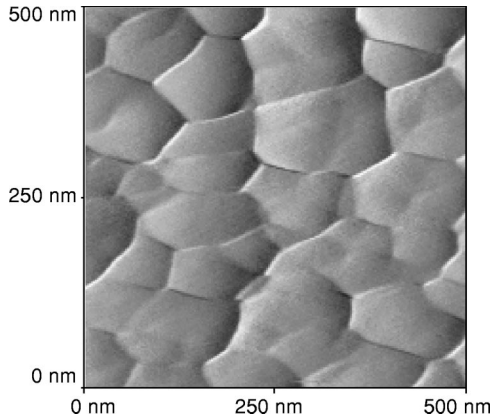

FIG. 1. AFM surface image of a STO1 film.

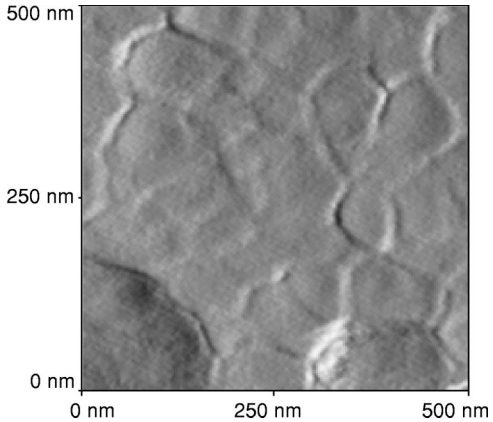

FIG. 2. AFM surface image of a STO3 film.

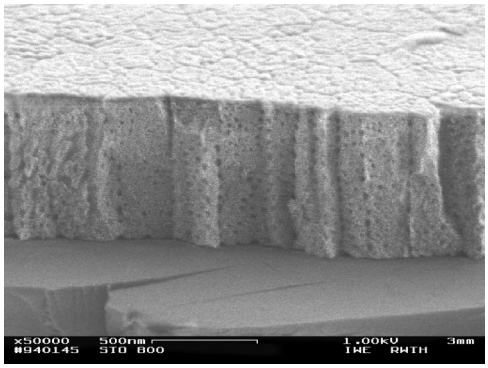

FIG. 3. Cross-sectional microstructure of a STO3 film, carried out by SEM.

resolution of 0.5 cm^{-1} in unpolarized light. Transmission geometry was chosen because it allows one to determine the TO1 mode parameters unambiguously in the case of a highly reflecting STO. The spectrometer was equipped with a liquid-He-cooled bolometer was used as the detector and polyethylene beam splitters of 6-, 50-, and 75-μm thicknesses. The samples were mounted in a continuous-flow cryostat Optistat CF and cooled down to 10 K. To increase the accuracy of the submillimeter data, the backward-wave-oscillator (BWO) technique (tunable coherent-source millimeter-submillimeter spectrometer) was employed.[40,41] This technique enabled us to measure independently the power transmittance and phase shift of the transmitted radiation in the 8–33-cm^{-1} frequency range. In both FTIR and BWO experimental setups the incident beam was normal to the sample surface, and therefore only the in-plane component of the dielectric response was probed.

C. Micro-Raman scattering

Raman scattering spectra of the films were taken using a Renishaw Raman microscope, where the 514-nm (2.14-eV) argon laser excitation with the spot size of 1–2 μm in diameter was used. A notch filter for suppresion the Rayleigh scattering did not allow us to resolve the spectra below 80 cm^{-1}. The samples were cooled in a nitrogen-cooled stage down to 80 K.

III. RESULTS AND EVALUATION

A. Fitting model

Transmittance spectra of the films were fitted to determine the TO mode parameters and to obtain the complex dielectric response function. Each sample was considered as a stack of two successive slabs, a film and a substrate (surrounded by vacuum), and the standard approach for the fit of a multilayer system was employed. The dielectric response function of each layer was evaluated using classical damped oscillator dispersion model,

$$\hat{\varepsilon}(\omega)=\varepsilon'(\omega)-i\varepsilon''(\omega)$$

$$=\varepsilon(\infty)+\sum_{j=1}^{n}\Delta\varepsilon_j\frac{\omega_{TOj}^2}{\omega_{TOj}^2-\omega^2+i\omega\gamma_{TOj}}, \qquad (1)$$

where $\varepsilon_\infty=n^2$ is the high frequency optical permittivity, ω_{TOj}, γ_{TOj} and $\Delta\varepsilon_j$ denote the eigenfrequency, damping, and dielectric strength of the jth transverse phonon mode, respectively. The values of $\hat{\varepsilon}(\omega)$ were used in the Fresnel formulas for complex transmission and reflection coefficients at the interface between neighboring media, and the complete transmittance of the two-layer system was computed by

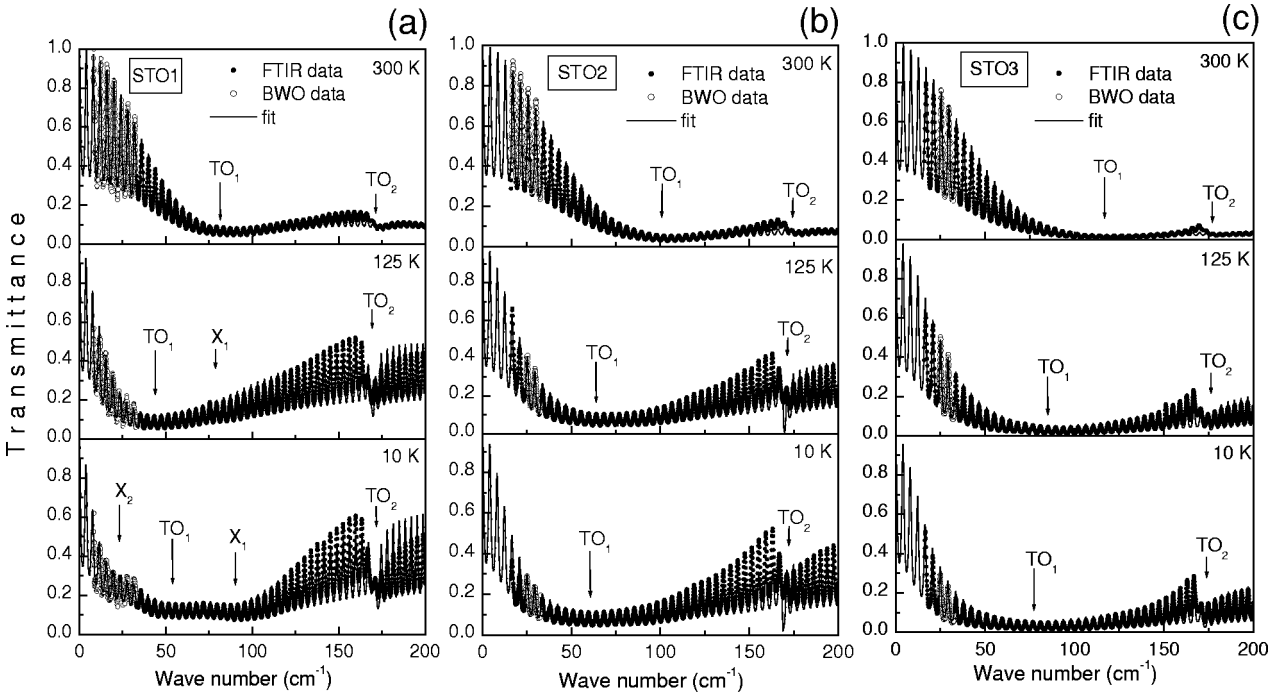

FIG. 4. FIR transmittance spectra of STO1 (a), STO2 (b) and STO3 (c) films at selected temperatures.

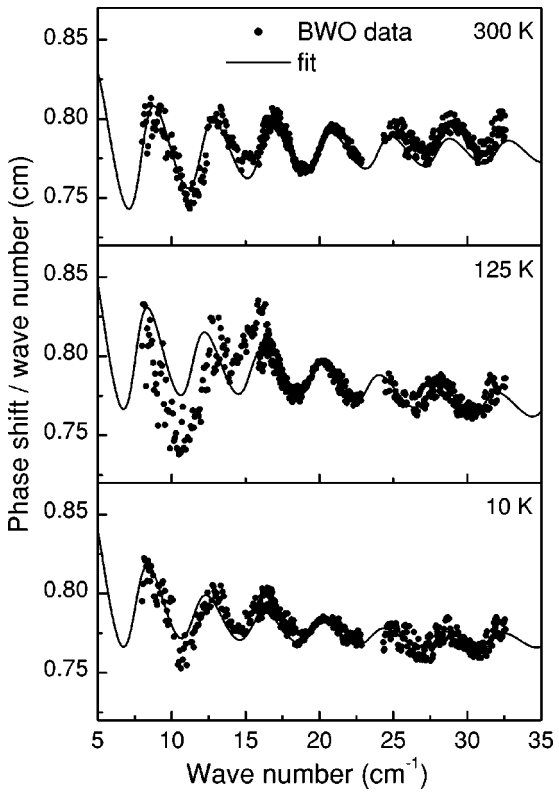

FIG. 5. Comparison of independently measured phase shift by BWO (full circles) with the curves, calculated using the parameters evaluated from the transmittance spectra fit. Results are obtained on STO1 film at selected temperatures.

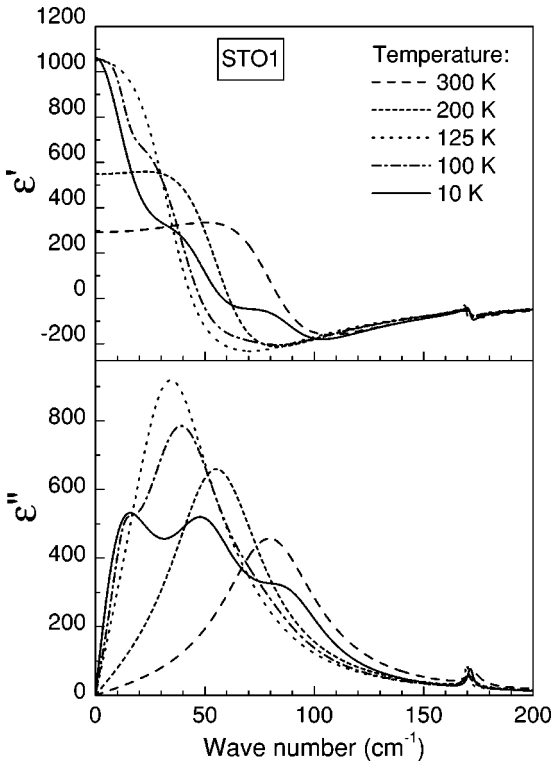

FIG. 6. Real and imaginary parts of dielectric permittivity of a STO1 film at selected temperatures, obtained from the fit of the transmittance spectra.

the transfer matrix formalism method[42] including interference phenomena. Trial and error fitting was used to optimize the agreement between all the data and fit parameters. For the STO films $\varepsilon_\infty = 5.3$ was taken as in the crystal,[38] and the parameters of the TO4 mode, lying above the transparency range, were evaluated from the fit of the room-temperature reflectance of the STO1 film ($\Delta\varepsilon_{\mathrm{TO4}} = 0.8$). These parameters were fixed independently of the temperature.

In order to reduce the ambiguity of the fit, the parameters of the substrate were obtained from an independent fit of transmittance spectra of a bare sapphire substrate for all the temperatures, and then fixed during the subsequent fits of film layers. The detailed analysis of these results on sapphire will be published elsewhere.[43] Here it should be mentioned that Al_2O_3 is partially transparent in the 0–300- and 0–400-cm^{-1} ranges at room and low temperatures, respectively. This enabled us to observe TO1 and TO2 phonon responses of the STO films in transmission mode in the whole 10–300-K temperature interval. The (0001) orientation of the substrate was chosen to avoid its optical anisotropy. This enabled us to fit the Fabry-Perot interference fringes appearing in the spectra due to the multiple reflection inside the 0.4-mm-thick substrate in an unpolarized IR beam.

A good agreement between the experiment and fit is seen from Fig. 4. The absorption of the TO1 mode is revealed by the broad temperature-dependent minimum. The weak second minimum at ~ 170 cm^{-1} indicates a weaker TO2 phonon. Its asymmetric spectral form suggests its coupling to the neighboring modes, and therefore the fit with independent oscillators is not perfect in this range. An agreement between the independently measured phase shift of the transmitted radiation and the one calculated with the parameters from the power transmittance fit (Fig. 5) proves the reliability of our simulation.

B. Results

Two striking effects were observed in the transmittance spectra of the STO1 film: a TO1 hardening below 125 K, and the appearance of absorption peaks (denoted by $X1$ and $X2$) on both sides of TO1 [Fig. 4(a)]. We have already reported the results obtained on this film in previous publications,[31,44] also indicating a minimum in the TO1 frequency temperature behavior. The low resolution of FTIR measurements in Ref. 31 did not allow us, however, to resolve the accompanying modes. In Ref. 44 the present FTIR results were used, but without the submillimeter data it was impossible to discern the $X2$ mode.

The spectra of STO2 and STO3 films are qualitatively different. The weak monotonous TO1 softening stops below 100 K [Figs. 4(b) and 4(c)], and no splitting is seen. The subsequent submillimetre measurements with only one BWO source (24–33 cm^{-1}) were carried out, enough to ensure the photometric accuracy of FTIR.

Real and imaginary part of the dielectric function evaluated for a STO1 film at selected temperatures is presented in Fig. 6. The static value of the permittivity changes very little below 125 K. Subsequent low-frequency maxima in the loss

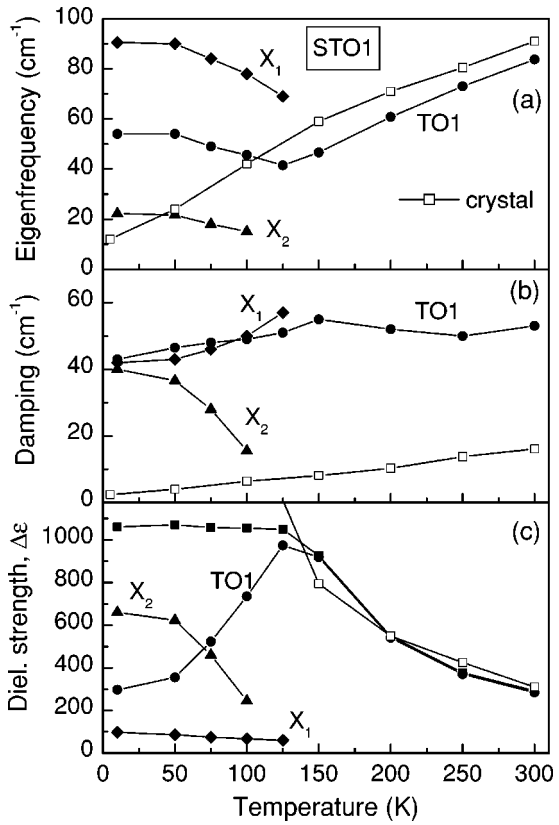

FIG. 7. Temperature dependence of the fit parameters of the lowest IR modes in a STO1 film in comparison with the parameters of TO1 mode in single crystal (Ref. 17).

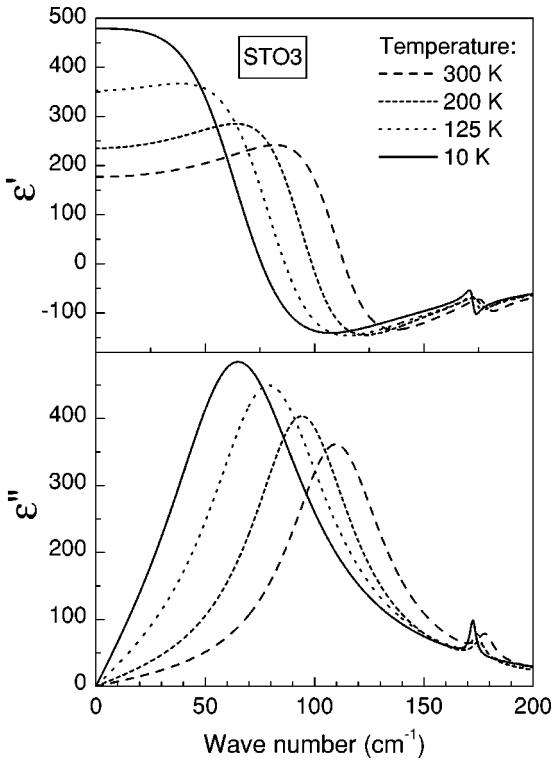

FIG. 8. Real and imaginary parts of the dielectric permittivity of a STO3 film at selected temperatures, obtained from the fit of the transmittance spectra.

spectra (ε'') indicate the position of $X1$, TO1, and $X2$ modes, respectively. Temperature dependence of their parameters is given in Fig. 7. Compared to single crystal, TO1 mode has reduced eigenfrequency in the 300–125-K temperature range (softens from 83 to 42 cm^{-1}), but below 125 K it hardens simultaneously with $X1$ and $X2$. Damping of all three modes is higher than in the crystal. The dielectric strengths of the $X1$ and $X2$ modes rise on cooling at the expense of TO1, leaving the total phonon contribution to the permittivity (sum of the dielectric strengths) constant below 125 K.

The FIR dielectric responses of STO2 and STO3 films differ substantially from that of STO1 (see Fig. 8 for the STO3 film). Compared to single crystal, the TO1 eigenfrequencies are markedly enhanced [see Fig. 9(a)]. Damping, whose room-temperature value is similar to that of STO1, increases on cooling below ~150 K [Fig. 9(b)]. The still higher TO1 frequency in STO3, compared with STO2, results in the lower permittivity of the former [Fig. 9(c)].

Micro-Raman spectra of the STO1 film are shown in Fig. 10. Symmetry forbidden TO2, TO4, and LO4 modes appear below 150 K and strengthen on further cooling. A very weak mode at ~260 cm^{-1}, corresponding to the silent TO3 frequency, is discerned below 100 K. Raman spectra of STO2 and STO3 films differ from those of STO1. The weak IR modes are detected even at room temperature and strengthen on cooling (Fig. 11 for STO3). The width (damping) of the TO2 and TO4 phonons in both STO2 and STO3 is almost twice as large as that in STO1. A weak peak at ~620 cm^{-1}, denoted by *Y*, has been seen in STO3. A weak increase of a signal is also found in this film at ~130 cm^{-1} below 150 K, which may be assigned to the *R*-point mode shifted from the single crystal value[9] of 143 cm^{-1}. Broad second-order features similar to those in single crystals are observed in STO2 and STO3 in the 230–300-cm^{-1} range.

IV. DISCUSSION

A. Lattice dynamics and dielectric properties

1. Quasiepitaxial STO1 film

STO1 film shows a higher tendency to the FE instability, as indicated by the reduced FE soft-mode frequency compared with single crystal. The minimum in its temperature dependence implies that a FE phase transition probably takes place at about 125 K. The activation of polar modes in the Raman spectra below this temperature confirms the loss of the inversion center. We have also checked it by the optical second harmonic generation signal in this film, which showed a non-zero intensity appearing just below ~130 K. The appearance of the $X1$ and $X2$ modes in the IR spectra could be then assigned to the AFD soft mode doublet, which becomes IR active due to the loss of inversion center. Here we assume that splitting of the FE soft mode itself, caused by the symmetry lowering, is too small to be resolved (in analogy with the single crystal[20] and ceramics[19]). Thus we suggest a simultaneous appearance of the FE and AFD order parameters in STO1 below 125 K. The fact that no *R*-point

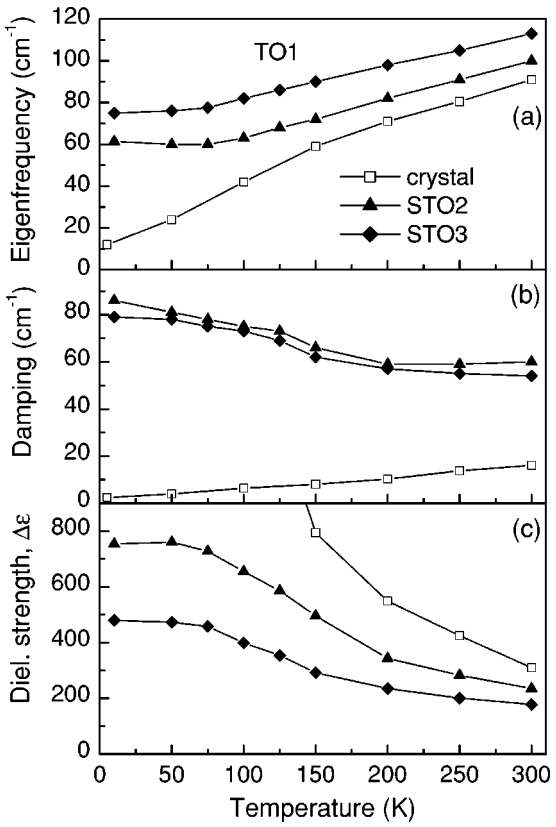

FIG. 9. Temperature dependence of the fit parameters of the TO1 modes in STO2 and STO3 films in comparison with corresponding parameters in a single crystal (Ref. 17).

modes were seen in our Raman spectra can be explained by their weakness in the thin film at temperatures above 80 K.

Provided that $X1$ and $X2$ modes represent the A_{1g} and E_g components of the AFD soft-mode doublet, respectively, their splitting ($\Delta\omega\sim 70$ cm^{-1}) is twice as large as in the crystal ($\Delta\omega\sim 35$ cm^{-1}). A part of the effect can be understood if one takes into account that all AFD and FE soft modes are now polar and should mutually couple, so that the TO1 mode, whose frequency lies inside the AFD doublet, will repel the components of the latter. In order to obtain bare, uncoupled frequencies of the AFD and FE soft modes, we performed an additional fit using a three coupled-oscillator model[45] for the soft-mode part of the spectra:

$$\Delta\hat{\varepsilon}(\omega) = \frac{S_0}{\omega_0^2-\omega^2-i\omega\gamma_0-\dfrac{\alpha_1^2(T)}{\omega_1^2-\omega^2+i\omega\gamma_1}-\dfrac{\alpha_2^2(T)}{\omega_2^2-\omega^2+i\omega\gamma_2}}. \quad (2)$$

Here we have assumed that oscillators representing the AFD soft-mode doublet with bare frequencies ω_1 and ω_2 have zero bare strengths. They couple to the FE soft mode with the bare frequency ω_0 and oscillator strength S_0 through the real coupling constants $\alpha_1(T)$ and $\alpha_2(T)$, respectively. S_0 therefore also represents the sum of the oscillator strengths

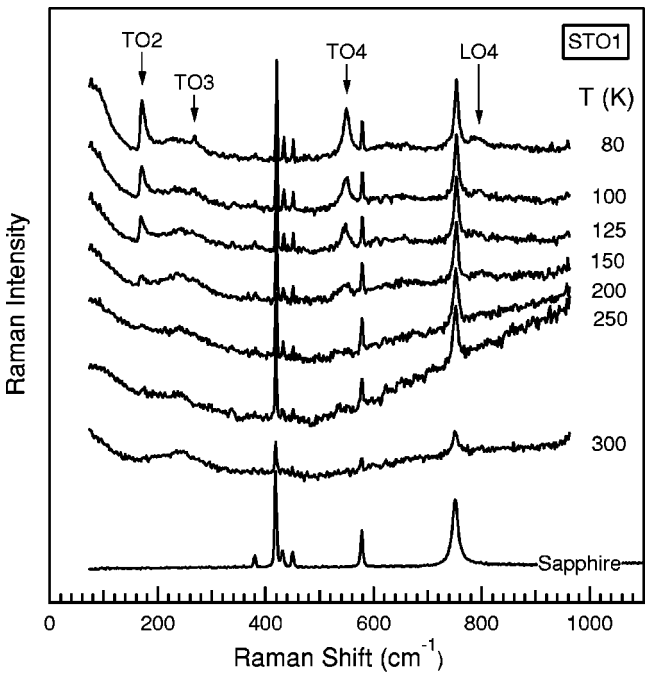

FIG. 10. Micro-Raman spectra of a STO1 film at selected temperatures.

of all three modes which is found to be temperature independent in the whole 10–300-K range:

$$S_0=\sum_j \omega_{TOj}^2(T)\Delta\varepsilon_j(T)\approx 2\times 10^6 \text{ cm}^{-2}. \quad (3)$$

This model demonstrates that without coupling to the FE soft mode, the splitting of the AFD soft mode would have

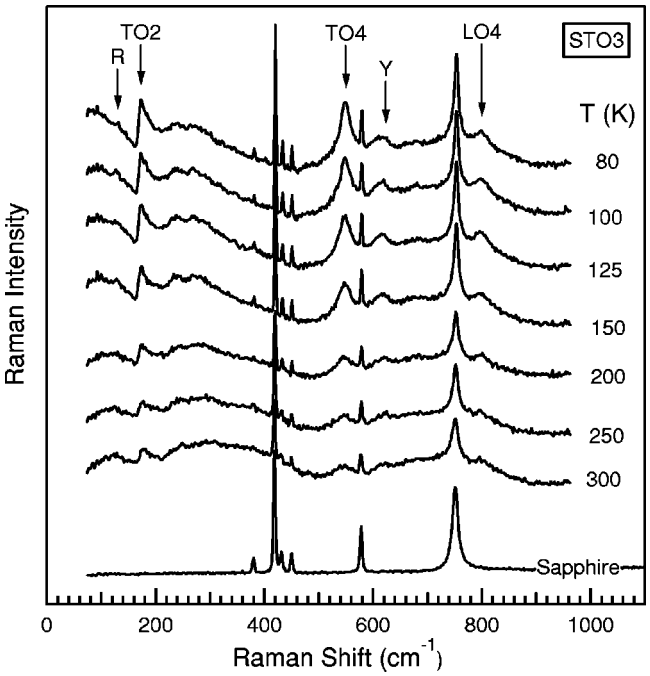

FIG. 11. Micro-Raman spectra of a STO3 film at selected temperatures.

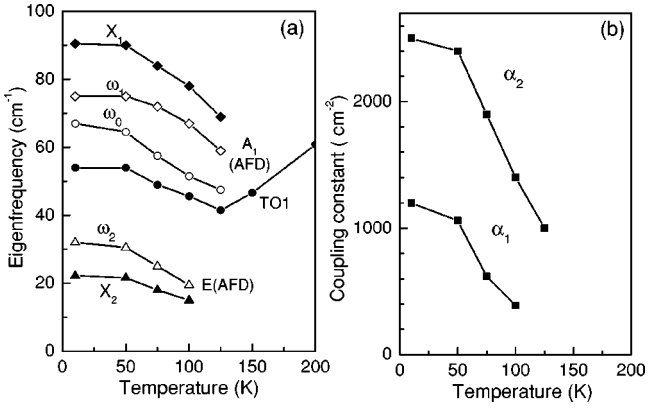

FIG. 12. Results of the fit of a STO1 film spectra by the model of three coupled oscillators: Bare eigenfrequencies $(\omega_0, \omega_1, \omega_2)$, depicted by empty symbols, are compared with the eigenfrequencies (full symbols) of the independent oscillator fit, i.e., influenced by the coupling. Coupling constants: α_1 between ω_1 and ω_0; α_2, between ω_2 and ω_0.

been only $\Delta\omega \sim 45$ cm^{-1} (Fig. 12), which is only by 10 cm^{-1} larger than in the crystal. It indicates a somewhat enhanced anisotropy in STO1 compared with the crystal. Both coupling constants increase on cooling, as well as all bare and coupled frequencies. This corresponds to the onset and increase of both order parameters. As all the frequencies as well as the coupling constants undergo stepwise changes at the transition, the transition has to be first order. This is natural to expect if the AFD transition triggers the FE one, or vice versa. The fact that $\alpha_2(T)$ is about twice as large as $\alpha_1(T)$ is consistent with the assumption that the spontaneous polarization lies in the film plane (see below), which corresponds to the crystallographic direction whose projection into all three crystal axes is statistically equivalent in unpolarized light. The calculated dielectric spectra within the coupled-mode model [Eq. (2)] practically coincide with those obtained by the independent-oscillator fit (Fig. 6).

The FE phase transition in the STO1 film is very probably connected with the residual stress. Pertsev *et al.* recently showed[46] that stress promotes the formation of a FE state with an out-of-plane orientation of the polarization in compressively stressed films and an in-plane polarization under the tensile stress. Our experiment on the STO1 film corresponds to the latter situation. In this respect it is worth mentioning that in crystals the uniaxial stress may also induce a FE state, but only along [001] and [110] directions.[47,48] The compression of the crystal in the [111] direction (equivalent of the tensile stress in the (111) plane) leads to a transformation into the nonpolar trigonal phase.[49] According to the single-crystal phase diagram,[50] T_a is increased up to ~125 K under an applied uniaxial [111] stress of 0.7 GPa (67 kg/mm^2) corresponding to our results. However, the appearance of the in-plane polarization in the film should indicate its symmetry reduction to monoclinic at least. Such a deviation from the single-crystal phase diagram must be caused by the fact that the free energy of films contains additional surface terms included into the calculations for the (100)-oriented STO film in Ref. 46. In the case of the (111) STO1 film the influence of the surface may be even stronger since, unlike a nonpolar (100) surface (composed of alternating stacks of two neutral layers, SrO and TiO_2), the (111) surface consists of two kinds of oppositely charged layers,[51] SrO_3^{4-} and Ti^{4+}.

We are aware of two studies where the onset of the ferroelectricity was directly manifested in pure STO films.[6,52] In both experiments the appearance of the spontaneous polarization was observed below 150 K. Despite the fact that the studied films were rather thick (200–500 nm) they were reported to exhibit a good epitaxiality. This allows us to consider epitaxiality as a necessary condition for the onset of macroscopic ferroelectricity in STO films, that may be accompanied by high permittivity values like those reported in Ref. 52 ($\varepsilon \simeq 1000$ at room temperature and a maximum of 5000 at 90 K).

2. Polycrystalline STO2 and STO3 films

The results on STO2 and STO3 films cannot be explained within the above-described model. Their main features are significant increase in ω_{TO1} and activation of IR modes in the Raman spectra in the whole studied temperature range. Similar effects were already observed in the previous IR (Refs. 17, 25, 26, 28, and 31) and Raman[53,54] experiments. One of the suggested explanations was the presence of oxygen vacancies.[53,54] In our opinion, however, point defects should cause weaker effects. Most probably, the activation of the forbidden modes in Raman spectra has the same origin as a similar effect in STO ceramics, which was assigned to the frozen dipole moment at grain boundaries.[19] Distortions on the grain boundaries were also discussed in Refs. 55 and 56 in connection with the appearance of an extra mode in the Raman spectra of BST films at about 620 cm^{-1}, which seems to correspond to our Y mode. Such distortions may result in a lower local permittivity, which in turn reduces the effective permittivity and enhances the effective FE soft mode frequency.[19] Moreover, the suggestion of the polar grain boundaries may explain the FE soft mode leveling off below ~100 K. That is, as the averaged structure becomes more polar, the AFD soft mode acquires a dipole moment through the coupling with the FE soft mode. This reduces the oscillator strength of the latter and its further softening, as far as the AFD soft modes harden on cooling below T_a. The increased effective damping of the FE soft mode at low temperatures might be understood as an envelope of all three overlapping IR active soft modes. In ceramics this effect was less pronounced than in our thin films: the effective permittivity of the 1–2-μm grained ceramics approached 10000 at low temperatures, and the relative intensity of the IR modes in Raman spectra was much weaker.[19] The reason for the more pronounced modifications of the dielectric response in films is obviously connected with their substantially larger grain-boundary volume fraction, caused by the smaller grain size. Our experience and literature analysis show that the mean grain size of a few hundred nm thick films usually does not exceed 100 nm, whereas the grain size in ceramics usually varies in the 1–50 μm range.

The decrease in the permittivity with decreasing grain size in the direction parallel to the probing field was demon-

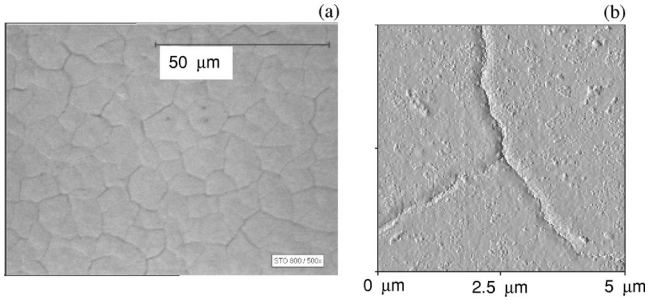

FIG. 13. Optical microscope (a) and AFM (b) views of a STO3 film surface, indicating the presence of cracks.

strated in BST (Ref. 57) as well as in STO films.[58] The microwave permittivity of an epitaxial 1-μm-thick STO film with 120-nm large grains achieved 5000 at low temperatures, while in a similar film with grains smaller than 50 nm it dropped down to 2000. As both these values still significantly exceed our results for STO2 and STO3, the presence of another factor strongly influencing the dielectric response in our films should be looked for. As both films differ in the soft-mode response, the searched property should differ in both the films.

To find it out we analyzed the morphology of our polycrystalline films. As described in Sec. II A both have a columnar structure with the porosity prevailing along the column boundaries. A look at the left side of Fig. 3 reveals the percolation of pores along the boundaries of several columns. It is natural to expect that such a percolated porosity may lead to crack formation. The careful observations by an optical microscope and AFM revealed such cracks, but only on the STO3 surface (Fig. 13). This is most probably the reason why the dielectric response in STO3 was more stiffened than in STO2.

To describe this effect quantitatively, we simplified the geometry of the model replacing porous column boundaries by straight gap surfaces separating neighboring columns, which in addition are covered by the layer of the grain-boundary region (Fig. 14). These gaps equally describe the percolated porosity on the column boundaries as well as possible cracks, both normal to the film surface and the probe electric field. Unlike isolated pores or parallel air gaps, such a series capacitance geometry exhibits much a stronger effect of the depolarizing field induced by the low permittivity layers inside the high-permittivity material.[59] The effective permittivity of such a system may be expressed in a way similar to the brick-wall model approach:[60]

$$\frac{1}{\varepsilon_{\mathrm{eff}}}=\frac{1-x_{\mathrm{gb}}-x_0}{\varepsilon_{\mathrm{cryst}}}+\frac{g_{\mathrm{gb}}x_{\mathrm{gb}}}{\varepsilon_{\mathrm{gb}}}+\frac{g_0x_0}{\varepsilon_0}. \tag{4}$$

Here $\varepsilon_{\mathrm{gb}}$ denotes a grain-boundary permittivity which is supposed to be lower then the permittivity of the grain bulk $\varepsilon_{\mathrm{cryst}}$. x_{gb} and x_o denote the volume fraction of grain boundaries and air gaps in the film, respectively, g_{gb} and g_o are geometric factors between 0 and 1, considering that only part of them in average is perpendicular to the electric field vector. Both these values are close to 1/2 in the case of our columnar grained structure. Equation (4) demonstrates that

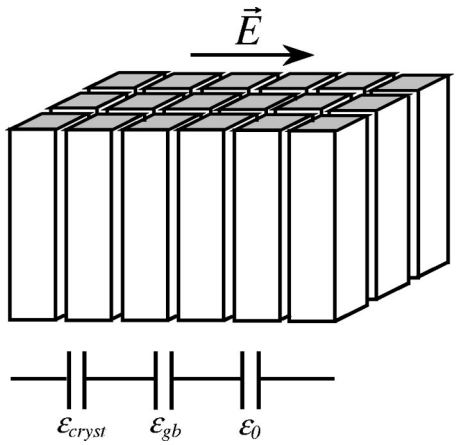

FIG. 14. Simplified sketch (brick-wall model) of STO2 and STO3 film morphologies (see the text), indicating their orientation with respect to the electric field vector in the present experiment. The series capacitance geometry is considered as the equivalent electric circuit.

unless $\varepsilon_{\mathrm{gb}}$ is essentially reduced in comparison with $\varepsilon_{\mathrm{cryst}}$, the key role in the reduction of the effective dielectric response belongs to the air gaps. It should be stressed that Eq. (4) is valid not only for the static properties, but also for the complex dynamic dielectric function as long as the electric field is homogeneous inside the grains, i.e., the IR radiation wavelength is much larger than the grain size (effective medium approximation[61–64]). This is certainly fulfilled in the case of the FE soft-mode response.

In Fig. 15 we illustrate how the percolated porosity of column boundaries influences the effective static permittivity and the corresponding FE soft-mode frequency (using the Lyddane-Sachs-Teller relation which is still valid for the effective quantities) provided the effect of typical (nonporous)

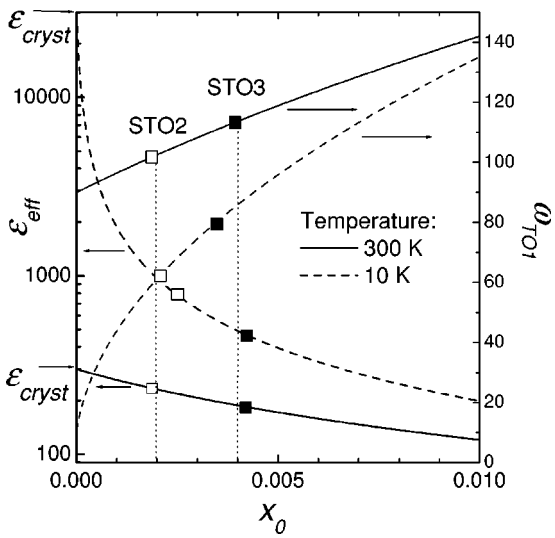

FIG. 15. Effective permittivity and corresponding FE soft-mode eigenfrequency as functions of volume fraction of air gaps between columnar grains, calculated using the brick-wall model. The parameters of our films are indicated on the curves in order to estimate their percolated porosity values.

TABLE II. Structural and FE soft-mode characteristics of STO films.

No.	Deposition method	Substrate	Thickness (nm)	Sr/Ti ratio	Stress-free lattice param. a_0 (nm)	Residual in-plane stress (GPa)	Cracks	Grain structure	Soft-mode frequency (cm^{-1}) (in-plane component)			Ref.
									300 K	100 K	10 K	
1	CSD	$(\bar{1}102)Al_2O_3$	160	1.00	-	tensile 1.5	no	100 nm, random orientation	93	60	65	31
2	CSD	$(\bar{1}102)Al_2O_3$	180	0.83	0.39066	tensile 0.9 ± 0.1	-	$\langle 110\rangle$ texture	95	71	72	28
3	PLD	$(\bar{1}102)Al_2O_3$	275	-	-	-	-	$\langle 110\rangle$ texture	95	63	64	17
4	MOCVD	$(0001)Al_2O_3$	290	0.97	0.39057	tensile 0.7 ± 0.1	no	$\sim$100 nm, $\langle 111\rangle$ highly oriented	83	45+78	22+54+91	STO1
5	PLD	$(0001)Al_2O_3$	330	-	-	-	-	-	98	-	50+100	27
6	CSD	$(0001)Al_2O_3$	360	1.05	0.39045	tensile 0.40 ± 0.05	no	$\sim$100 nm, weak $\langle 100\rangle$ texture	100	63	61	STO2
7	CSD	$(\bar{1}102)Al_2O_3$	440	0.94	-	-	yes	$\sim$100 nm, $\langle 100\rangle$ texture	111	76	75	31
8	CSD	$(0001)Al_2O_3$	680	0.96	0.39031	tensile 0.15 ± 0.03	yes	$\sim$100 nm, weak $\langle 100\rangle$ texture	113	82	75	STO3
9	CSD	SiO_2 glass	70–800	-	-	-	yes	-	110	-	-	29
10	PLD	(001) MgO	90–1070	-	-	-	-	-	102	-	-	67
11	PLD	$SrRuO_3+SrTiO_3$	2000	-	-	-	-	-	99	68	62	25
	Ceramics	-	-	1.00	0.39058	-	no	1–2 μm	94	46	$\sim$15	19
	Crystal	-	-	-	0.39059	no	no	no	87-91	42	7.8+16.5 $\sim$11	7,15–17,20

grain boundaries and localized pores is neglected. The calculations correspond to the above described model [Eq. (4)] with $g_0=1/2$ and $x_{gb}=0$. The result is not very sensitive to the g_o factor and about 0.2 vol% of air gaps ($x_0=2\times10^{-3}$) appears to be enough to reduce static permittivity from 300 to 240 and increase the soft-mode frequency from 90 to 100 cm^{-1} at room temperature. At 10 K the same porosity reduces the static permittivity from 30000 to less then 1000, and increases the soft mode frequency from 11 to 62 cm^{-1}. These values are quite close to those obtained for our STO2 film. As demonstrated in Fig. 13, twice as high a volume fraction of the gaps describes our results for STO3. A rough estimate using the averaged density of the cracks observed on the STO3 surface shows that their thickness should not exceed 10 nm. This number looks quite realistic. However, it should be pointed out that the cracks developing perpendicular to the film surface should significantly influence only the in-plane component of the dielectric response probed in our experiment. The standard Hz-MHz dielectric techniques probe the out-of-plane response, for which the perpendicular cracks may result in an electrical short circuiting (due to the diffusion of the electrode through the cracks) rather than in a substantial reduction of the permittivity. The former fact is also well known to appear if one uses large area electrodes. In the latter geometry the main role in the dielectric response will be played by layers parallel to the surface, such as interface (dead) layers[65] and grain boundaries parallel to the film plane.

B. Analysis of the factors affecting the soft-mode dynamics and dielectric properties

Finally we are going to summarize the results for the soft-mode behavior of STO films, complementing data of the present experiment with the earlier reported results. This illustrates to what extent the effects demonstrated above are applicable to other films and their role among other factors. Available characteristics of STO thin films whose soft-mode behavior has been studied by means of FIR experiment (in-plane response) are presented in Table II. The included data are either taken from the literature or were evaluated for the samples we have at our disposal. All characteristics except for the soft-mode frequency are measured at room temperature only.

The Sr/Ti ratio is one of the available stoichiometry criteria. No pronounced correlation between its value and soft mode behavior is seen. Unlike the results in SBT (Ref. 3) in nonstoichiometric film No. 2 with a substantial Ti excess, the soft mode is only slightly less temperature dependent. The stress-free lattice parameter can also be considered as a stoichiometry characteristics, as its enhancement is often connected with the presence of oxygen vacancies.[66] In the films in Table II, for which this parameter was evaluated, it is very close to the single-crystal value. This allows us to expect a rather small oxygen vacancy concentration in all the studied films.

In films where the residual stress was estimated, it appeared to be tensile in the plane of the film in spite of the fact

that the interatomic spacing of STO is substantially larger than the corresponding distance in Al_2O_3 for all orientations used. This can be understood considering the larger thermal expansion coefficient of STO compared with the Al_2O_3 substrate.[38] Assuming that the film is completely relaxed at the deposition temperature, the substrate, more slowly shrinking on cooling than the film, causes its stretching, which for a higher thickness may relax via cracks.

The films in Table II are listed according to their thicknesses, film No. 1 being the thinnest one. This enables us to follow the thickness dependence of their properties. First of all, the residual stress decreases with increasing film thickness: the thicker films are more stress relaxed. In films thicker than 400 nm, the stress relaxation results in the appearance of the cracks, which may be observed by an optical microscope. The crack appearance directly correlates with the increase of the FE soft-mode frequency that shows that the air gaps are the main factor influencing the dielectric response of these films.

Film No. 4 (STO1) lies apart from the general tendency. It is the only epitaxial film from Table II possessing almost perfect grain ordering. We see it as the main reason why the effect of the residual stress was revealed only in this film.

V. CONCLUSIONS

Epitaxiality seems to be a decisive condition enabling an appearance of the stress-induced FE phase transition in STO films. The present experiment shows that the polariztion appears in the direction parallel to the tensile stress, as predicted in Ref. 46.

No strain effect was revealed on the polycrystalline films. They demonstrated a weakening of the ferroelectric instability, which was concluded from the enhanced values of the FE soft-mode frequency and its leveling off below 100 K. On the other hand, their Raman spectra exhibited a presence of symmetry forbidden IR modes in the whole studied 10–300-K temperature range. The porosity and acentricity of the grain boundaries are suggested as the main reasons for such a behavior, respectively. The effective dielectric response of the columnar grained films was estimated within the series capacitance geometry, that allowed to take into account the strong depolarizing field induced by the percolated porosity normal to the probing electric field. So far the influence of the porosity on the thin film dielectric properties has not been discussed in the literature, *a priori* assuming it to be negligible in the high quality films. We have shown, however, that pores tend to percolate in certain layers at the grain boundaries, and that much less than 1% of such a porosity is enough to drastically reduce the dielectric response of the high-permittivity materials. Thicker films demonstrate worse in-plane dielectric characteristics (higher FE soft-mode frequency) due to the increasing tendency to the crack formation. As long as this experiment was performed within a noncontact geometry and with electric field parallel to the film surface, the effect of interfacial layers was not studied in the present work.

ACKNOWLEDGMENTS

The authors are grateful to A.K. Tagantsev and I. Rychetský for helpful discussions, as well as to J. Kroupa for performing the SHG measurements and to V. Peřina for carrying out RBS studies. The STO1 sample was provided by J. Lindner. The work was supported by the Grant Agency of the Czech Rep. (Project Nos. 202/01/0612 and 202/02/0238), Academy of Sciences of the Czech Rep. (Project No. AVOZ1-010-914), Czech Ministry of Education (Project No. COST OC 525.20/00 and OC 528.001/01), and by the Deutsche Forschungsgemeinschaft (DFG) via GO 976/1.

*Permanent address: Institut of General Physics, RAS, 119991 Moscow, Russian Federation.

[1] B.M. Gol'tsman, V.V. Lemanov, A.I. Dedyk, L.T. Ter-Martirosyan, and S.F. Karmanenko, Fiz. Tverd. Tela (Leningrad) **38**, 2493 (1996) [Phys. Solid State **38**, 1368 (1996)].

[2] R. Waser, Integr. Ferroelectr. **15**, 39 (1997).

[3] S.K. Streiffer, C. Basceri, C.B. Parker, S.E. Lash, and A.I. Kingon, J. Appl. Phys. **86**, 4565 (1999).

[4] H.-Ch. Li, W. Si, A.D. West, and X.X. Xi, Appl. Phys. Lett. **73**, 464 (1998).

[5] Yu.A. Boikov, Z.G. Ivanov, E. Olsson, and T. Claeson, Physica C **282-287**, 111 (1997).

[6] D. Galt, J.C. Price, J.A. Beall, and R.H. Ono, Appl. Phys. Lett. **63**, 3078 (1993).

[7] A.S. Barker, Jr. and M. Tinkham, Phys. Rev. **125**, 1527 (1962).

[8] K.A. Müller, W. Belinger, and E. Tosatti, Z. Phys. B: Condens. Matter **84**, 277 (1991).

[9] P.A. Fleury, J.F. Scott, and J.M. Worlock, Phys. Rev. Lett. **21**, 16 (1968).

[10] G. Shirane and Y. Yamada, Phys. Rev. **177**, 858 (1969).

[11] G. Rupprecht and R.O. Bell, Phys. Rev. **125**, 1915 (1962).

[12] K. Bethe, Philips Res. Rep. **2**, 1 (1970).

[13] C.H. Perry, B.N. Khanna, and G. Rupprecht, Phys. Rev. **135**, A408 (1964).

[14] J.D. Axe, Phys. Rev. **157**, 429 (1967).

[15] J.L. Servoin, Y. Luspin, and F. Gervais, Phys. Rev. B **22**, 5501 (1980).

[16] K. Kamaras, K.-L. Barth, F. Kilmann, R. Henn, M. Reedyk, C. Thomsen, J. Kircher, P.L. Richards, and J.-L. Stehle, J. Appl. Phys. **78**, 1235 (1995).

[17] I. Fedorov, V. Železný, J. Petzelt, V. Trepakov, M. Jelínek, V. Trtík, M. Černanský, and V. Studnička, Ferroelectrics **208-209**, 413 (1998).

[18] H.-M. Christen, J. Mannhart, E.J. Williams, and C. Gerber, Phys. Rev. B **49**, 12095 (1994).

[19] J. Petzelt, T. Ostapchuk, I. Gregora, I. Rychetský, S. Hoffmann-Eifert, A.V. Pronin, Y. Yuzyuk, B.P. Gorshunov, S. Kamba, V. Bovtun, J. Pokorný, M. Savinov, V. Porokhonskyy, D. Rafaja, P. Vaněk, A. Almeida, M.R. Chaves, A.A. Volkov, M. Dressel, and R. Waser, Phys. Rev. B **64**, 184111 (2001).

[20] A. Yamanaka, M. Kataoka, Y. Inaba, K. Inoue, B. Hehlen, and E. Courtens, Europhys. Lett. **50**, 688 (2000).

[21] T. Sakudo and H. Unoki, Phys. Rev. Lett. **26**, 851 (1971).

[22] R.P. Lowndes and A. Rastogi, J. Phys. C **6**, 932 (1973).

[23] G.V. Belokopytov, Ferroelectrics **168**, 69 (1995).
[24] K. Ikuta, Y. Umeda, and Y. Ishii, J. Appl. Phys. **34**, L1211 (1995).
[25] A.A. Sirenko, C. Bernhard, A. Golnik, A.M. Clark, J. Hao, W. Si, and X.X. Xi, Nature (London) **404**, 373 (2000).
[26] X.X. Xi, A.A. Sirenko, I.A. Akimov, A.M. Clark, J.H. Hao, and W. Si, Integr. Ferroelectr. **28**, 247 (2000).
[27] V. Železný, J. Petzelt, and K. Kämmer, J. Korean Phys. Soc. **32**, S1615 (1998).
[28] J. Petzelt, T. Ostapchuk, S. Kamba, I. Rychetský, M. Savinov, A. Volkov, B. Gorshunov, A. Pronin, S. Hoffmann, R. Waser, and J. Lindner, Ferroelectrics **239**, 117 (2000).
[29] J. Buršík, P. Vaněk, V. Studnička, T. Ostapchuk, E. Buixaderas, J. Petzelt, R. Krupková, B. Březina, and V. Peřina, Ferroelectrics **241**, 191 (2000).
[30] J. Petzelt and T. Ostapchuk, Ferroelectrics **249**, 81 (2001).
[31] J. Petzelt, T. Ostapchuk, I. Gregora, S. Hoffmann, J. Lindner, D. Rafaja, S. Kamba, J. Pokorný, V. Bovtun, V. Porokhonsky, M. Savinov, P. Vaněk, I. Rychetský, V. Peřina, and R. Waser, Integr. Ferroelectr. **32**, 11 (2001).
[32] P. Grosse, Trends in Analytical Chem. **8**, 222 (1989).
[33] J. Petzelt, T. Ostapchuk, and S. Kamba, in *Defects and Surface-Induced Effects in Advanced Perovskites*, Vol. 77 of *NATO Science Series 3: High Technology*, edited by G. Borstel, A. Krumnis, and D. Millers (Kluwer, Dordrecht, 2000), p. 233.
[34] F. Weiss, J. Lindner, J.-P. Sénateur, C. Dubordieu, V. Galindo, M. Audier, A. Abrutis, M. Rosina, K. Frohlich, W. Haessler, S. Oswald, A. Figueras, and J. Santiso, Surf. Coat. Technol. **133**, 191 (2000).
[35] S. Hoffmann, U. Hasenkox, R. Waser, C.L. Jia, and K. Urban, in *Epitaxial Oxide Thin Films III*, edited by D. G. Schlom, Chang-Beam Yeom, M. E. Hawley, C. M. Foster, and J. S. Speck, MRS Symposia Proceedings No. 474 (Materials Research Society, Pittsburgh, 1977), p. 9.
[36] C.L. Jia, K. Urban, S. Hoffmann, and R. Waser, J. Mater. Res. **13**, 2206 (1998).
[37] E.D. Palik, *Handbook of Optical Constants of Solids II* (Academic Press, Boston, 1991), p. 1042.
[38] *Crystal and Solid State Physics*, edited by K.-H. Hellwege, Landolt-Börnstein, New Series, Group III, Vol. 16, Pt. a (Springer-Verlag, Berlin, 1981), p. 155.
[39] D. Rafaja, J. Kub, D. Šimek, J. Lindner, and J. Petzelt, Thin Solid Films (to be published).
[40] G. Kozlov and A. Volkov, in *Millimeter and Submillimeter Wave Spectroscopy of Solids*, edited by G. Gruner (Springer, Berlin, 1998), p. 51.
[41] A. Pashkin, P. Kužel, J. Petzelt, B. Gorshunov, and M. Dressel, Ferroelectrics **272**, 219 (2002).
[42] O.S. Heavens, Rep. Prog. Phys. **XXIII**, 1 (1960).
[43] T. Ostapchuk, J. Petzelt, and V. Železný (unpublished).
[44] J. Petzelt and T. Ostapchuk, Ferroelectrics **267**, 93 (2002).
[45] J. Petzelt, F. Smutny, V. Katkanant, F.G. Ullman, J.R. Hardy, A.A. Volkov, G.V. Kozlov, and S.P. Lebedev, Phys. Rev. B **30**, 5172 (1984).
[46] N.A. Pertsev, A.K. Tagantsev, and N. Setter, Phys. Rev. B **61**, R825 (2000). N.A. Pertsev, A.K. Tagantsev, and N. Setter, *ibid.* **65**, 219901(E) (2002).
[47] W.J. Burke and R.J. Pressley, Solid State Commun. **9**, 191 (1971).
[48] H. Uwe and T. Sakudo, Phys. Rev. B **13**, 271 (1976).
[49] W.J. Burke and R.J. Pressley, Solid State Commun. **7**, 1187 (1969).
[50] K.A. Müller, W. Berlinger, and J.C. Slonczewski, Phys. Rev. Lett. **25**, 734 (1970).
[51] S. Sekiguchi, M. Fujimoto, M. Nomura, S.B. Cho, J. Tanaka, T. Nishihara, M.-G. Kang, and H.-H. Park, Solid State Ionics **108**, 73 (1998).
[52] D. Fuchs, C.W. Schneider, R. Schneider, and H. Rietschel, J. Appl. Phys. **85**, 7362 (1999).
[53] V.I. Merkulov, J.R. Fox, H.-Ch. Li, W. Si, A.A. Sirenko, and X.X. Xi, Appl. Phys. Lett. **72**, 3291 (1998).
[54] A.A. Sirenko, I.A. Akimov, J.R. Fox, A.M. Clark, H.-Ch. Li, W. Si, and X.X. Xi, Phys. Rev. Lett. **82**, 4500 (1999).
[55] R. Naik, J.J. Nazarko, C.S. Flattery, U.D. Venkateswaran, V.M. Naik, M.S. Mohammed, G.W. Auner, J.V. Mantese, N.W. Schubring, A.L. Micheli, and A.B. Catalan, Phys. Rev. B **61**, 11 367 (2000).
[56] Yu.I. Yuzyuk, V.A. Alyoshin, I.N. Zakharchenko, E.V. Sviridov, A. Almeida, and M.R. Chaves, Phys. Rev. B **65**, 134107 (2002).
[57] T. Kuroiwa, Y. Tsunemine, T. Horikawa, T. Makita, J. Tanimura, N. Mikami, and K. Sato, Jpn. J. Appl. Phys. **33**, 5187 (1994).
[58] M.J. Dalberth, R.E. Strauber, J.C. Price, and C.T. Rogers, Appl. Phys. Lett. **72**, 507 (1998).
[59] I. Rychetský, J. Petzelt, and T. Ostapchuk, Appl. Phys. Lett. **81**, 4224 (2002).
[60] M.H. Frey, Z. Xu, P. Han, and D.A. Payne, Ferroelectrics **206-207**, 337 (1998).
[61] G.L. Carr, S. Perkowitz, and D.B. Tanner, in *Infrared and Millimeter Waves*, edited by K.J. Button (Academic Press, Orlando, 1985) Vol. 13. p 172.
[62] W. Theiss, in *Festkörperprobleme*, *Advances in Solid State Physics*, edited by R. Helbig (Vieweg, Braunschweig, 1994), Vol. 33, p. 149.
[63] O. Hudák, I. Rychetský, and J. Petzelt, Ferroelectrics **208-209**, 429 (1998).
[64] I. Rychetský, O. Hudák, and J. Petzelt, Phase Transitions **67**, 725 (1999).
[65] C. Basceri, S.K. Steiffer, and A.I. Kingon, J. Appl. Phys. **82**, 2497 (1997).
[66] W.J. Kim, W. Chang, S.B. Quadri, J.M. Pond, S.W. Kirchoefer, and J.S. Horwitz, Appl. Phys. Lett. **76**, 1185 (2000).
[67] T.K. Song, J.S. Ahn, H.S. Choi, T.W. Noh, and S.-I. Kwun, J. Korean Phys. Soc. **30**, 623 (1997).